journal

J. Am. Ceram. Soc., 77 [1] 165–71 (1994)

Reaction Hot Pressing of α′- and β′-SiAlON Ceramics

Shyh-Lung Hwang* and I-Wei Chen*

Department of Materials Science and Engineering, University of Michigan, Ann Arbor, Michigan 48109

Hot pressing kinetics of α-Si_3N_4, AlN, Al_2O_3, and Y_2O_3 powder mixtures forming α′- and β′-SiAlONs have been studied. Densification proceeds in two steps, first by a small shrinkage upon ternary eutectic oxide melting (SiO_2–Al_2O_3–Y_2O_3) at 1340°C, followed by a massive particle rearrangement and further shrinkage at higher temperature when nitride dissolution begins. With better wettability, AlN initially traps the oxide melt and delays densification. In addition, the preferential dissolution of AlN at 1450°C enriches the melt composition in Al, triggering transient precipitation of supersaturated β′-SiAlON. Full densification is readily achieved at 1550°C without complete α-Si_3N_4 conversion.

I. Introduction

Hot pressing is a reliable technique for the fabrication of high-density and high-strength nitrogen ceramics. Typically, sintering aids such as MgO, Y_2O_3, or Li_2O are used in hot pressing of silicon nitride.[1–5] These oxide additives first react with the residual silica on the silicon nitride powder surface to form a eutectic melt which facilitates densification of the powder compact during hot pressing. Upon cooling, this eutectic melt remains on the silicon nitride grain boundary as a glassy phase which has detrimental effects on both the chemical and mechanical properties of silicon nitride based ceramics at elevated temperatures.[6–11]

SiAlONs are the solid solutions of α-Si_3N_4 or β-Si_3N_4 with O, Al, and some other metal ions M. The general formula is $M_pSi_{12-(m+n)}Al_{(m+n)}O_nN_{16-n}$ for α′-SiAlON and $Si_{6-x}Al_xO_xN_{8-x}$ for β′-SiAlON, where the subscripts p, m, n, and x are variables within their respective solubility range. To fabricate these materials, the starting powder compacts usually contain Si_3N_4, Al_2O_3, AlN, and other metal oxides such as Y_2O_3. The low-temperature eutectic liquid that forms and aids densification can be later incorporated into the silicon nitride lattice to form α′- or β′-SiAlON.[12,13] Thus, the amount of residual grain boundary glassy phase after fabrication is drastically reduced. Hot pressing in this case is called reaction hot pressing.

The reaction hot pressing studies were mostly limited to β′-SiAlON in relatively simple systems.[4,14–20] Two general conclusions can be drawn from these studies. First, the composition with a higher x value usually has a higher shrinkage rate. Second, the densification rate increases rapidly with the amount of excess oxides beyond those required to form β′-SiAlON. These results can be attributed to either an increasing amount of liquid phase at the hot pressing temperature or a modification of overall liquid composition toward the SiO_2 corner. It has also been accepted that dissolution/reprecipitation is the primary densification mechanism in hot pressing of Si_3N_4/SiAlONs.[1,2,6] On the other hand, although reaction pathways in pressureless sintering in systems such as SiO_2–AlN, Si_3N_4–AlN–SiO_2, and Si_3N_4–AlN–Al_2O_3 forming β′-SiAlON are well established,[21–23] they have not been identified in more complicated systems outside the Si_3N_4–AlN–SiO_2–Al_2O_3 plane. Since the kinetic pathway may depend on both the (equilibrium) phase relationship and the physical/chemical characteristics (such as wettability, surface area, etc.) of the powders, it needs to be established in a more general way for those systems of current interest. A basic understanding of this aspect is ultimately important for the fabrication and microstructural control of SiAlON ceramics.

The present work was motivated by the above consideration and our interest in developing superplastic SiAlONs.[24–26] For the latter application, low densification temperature is desired in order to obtain as fine a microstructure as possible.[24] This has been achieved for a variety of α′-, β′-, and (α + β)-SiAlONs in the Y-Si-Al-N-O system by reaction hot pressing at 1550°C. In this paper, we report the central observations which bear on the kinetic pathways of SiAlON formation using multicomponent powders (Si_3N_4, AlN, Al_2O_3, and Y_2O_3). For comparison, simple Si_3N_4–Al_2O_3–Y_2O_3 ternaries and other model systems are also investigated. The detailed microstructural characterization and mechanical forming characteristics of these superplastic SiAlONs will be published elsewhere.

II. Experimental Procedure

(1) Composition

The compositions of materials investigated here are represented graphically in Figs. 1 and 2. The first set of compositions lies on the Si_3N_4–Al_2O_3–Y_2O_3 plane and forms the reference point for composition with superplastic SiAlONs. The second set lies on the Si_3N_4–Al_2O_3:AlN–YN:3AlN plane and contains, in equilibrium, α′- and β′-SiAlON phase assemblages of various proportions. The latter compositions have been extensively utilized in our research to obtain superplastic SiAlONs. Since the compositions on the Si_3N_4–Al_2O_3:AlN–YN:3AlN plane can be represented by the formula $Y_{m/3}Si_{12-(m+n)}Al_{m+n}O_nN_{16-n}$, we use (m, n) to designate the composition in the second set. For instance, composition 0610 stands for $m = 0.6$ and $n = 1.0$. These compositions can be subdivided into four groups, A through D, each of which has a fixed Al_2O_3:AlN/Y_2O_3:9AlN ratio. Graphically, they correspond to a set of straight lines extending from the Si_3N_4 corner, as shown in Fig. 2. The total amount of additives including AlN, Y_2O_3, and Al_2O_3 ranges from 17 to 50 wt%.

(2) Powder Processing

The compositions were prepared in 40-g batches from their starting powders (α-Si_3N_4, UBE, E10; AlN, Tokuyama Soda Co., Ltd., Type F; Al_2O_3, Sumitomo Chemical America Inc., AKP50; and Y_2O_3, Aldrich Chemical Co., Inc.). The oxygen contents (in wt%) were 1.48% (Si_3N_4) and 0.98% (AlN). The purity of Al_2O_3 was 99.995% and that of Y_2O_3 was 99.9%. Compensation was made in the composition calculations for the presence of surface oxides in the starting nitride powders. The powders were attrition milled in 2-propanol in a Teflon-lined steel jar of 0.7-L size using 500 g of high-purity alumina milling balls (2 mm in diameter) for 2 h at a speed of 900 rpm. The

M. Harmer—contributing editor

Manuscript No. 194606. Received May 3, 1993; approved September 17, 1993.
Supported by the U.S. National Science Foundation under Grant No. DDM-90-24975.
*Member, American Ceramic Society.
*Now at Oak Ridge National Laboratory, Metals and Ceramics Division, Oak Ridge, Tennessee.

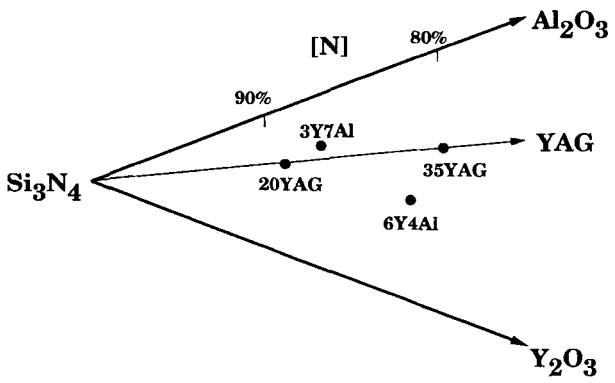

Fig. 1. Compositions studied on Si_3N_4–Al_2O_3–Y_2O_3 plane.

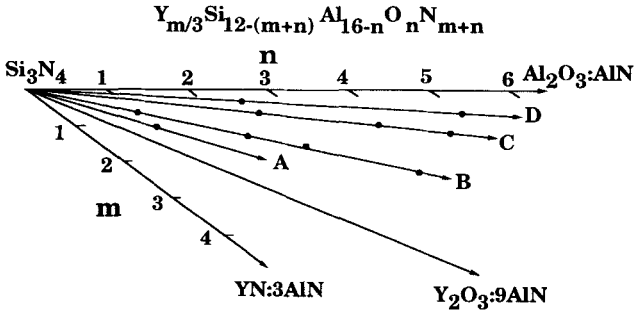

Fig. 2. Compositions studied on Si_3N_4–Al_2O_3:AlN–YN:3AlN plane.

amounts of surface oxides in the starting nitride powders and alumina pick-up from the alumina balls were compensated for in the formulation of the initial powder batches. After milling, the powder–2-propanol slurry was stirred in a Teflon beaker using a magnetic stirrer and dried under an infrared lamp at about 80°C.

(3) Hot Pressing

Dense specimens were obtained by hot-pressing 14-g charges in a graphite resistance furnace using a high-purity graphite die under 1 atm of nitrogen. The powder was first cold-pressed at a load of 27 MPa, then loaded into the hot-press. The heating schedule was 25°C/min from room temperature to 1000°C followed by 15°C/min to 1550°C. The holding time at 1550°C varied between 17 and 30 min depending on the shrinkage behavior of the powder compact. A load of 27 MPa was applied at all times during heating, pressing, and cooling when the temperature exceeded 1000°C. The shrinkage of powder compacts, as represented by the pressing ram travel, was monitored by an LVDT. (The contribution of the thermal expansion of the entire loading train was subtracted from the travel data, which have an accuracy of 0.1 mm.) The initial and final thicknesses of the compact were around 8 and 3.3 mm, respectively, and varied slightly with composition at the same 14-g weight. Hot pressing was repeated for one-third of the compositions from which the data reproducibility was verified.

(4) Characterization

Standard characterization using X-ray diffraction (XRD), scanning electron microscopy (SEM), and transmission electron microscopy (TEM) was performed to clarify phase and microstructural evolution. In addition, wetting angles between the SiO_2–Al_2O_3–Y_2O_3 ternary eutectic melt and Si_3N_4 and AlN were measured to understand the initial steps in liquid-phase reactions. These characterization techniques will be described in more detail in appropriate places in the next section.

III. Results

(1) Shrinkage Behavior

(A) Si_3N_4–Al_2O_3–Y_2O_3: The shrinkage curves for the four materials selected from the Si_3N_4–Al_2O_3–Y_2O_3 plane (Fig. 1) are shown in Fig. 3. Also shown is the curve from another material containing AlN which will be discussed later. Without AlN, all the materials have similar shrinkage behavior despite their different compositions. Common distinct features include a first shrinkage step at 1340°C, followed by a second shrinkage step starting at 1450°C. These steps are identified by the onset of a fast shrinkage. Each step of fast shrinkage is then followed by a period of slow shrinkage, giving an s-shaped appearance overall.

The first shrinkage step is associated with initial compaction of the powder upon the formation of the SiO_2–Al_2O_3–Y_2O_3 ternary eutectic liquid, which is 1350°C.[27] This is the lowest temperature for liquid formation and is independent of the starting powder composition. Since the amount of SiO_2 ranges from 1.56 to 1.94 wt% in these materials, the amount of eutectic melt is small and can cause only a small shrinkage (≈4%). At higher temperature, e.g., 1450°C, the liquid-phase region expands slightly[27] around the eutectic point but is still largely independent of the initial composition. As will be shown later, the second shrinkage step corresponds to the dissolution of Si_3N_4 powder into the nearly ternary eutectic melt. The total amount of volume shrinkage achieved, typically ≈40 vol%, is representative of densification of a liquid-containing powder compact.[28]

Given the above general characteristics which are composition independent, it is remarkable to see that a partial substitution of Si_3N_4 by AlN causes a shift of the shrinkage curve to a higher temperature. An example of this is observed in the 20YAG + 15AlN material as shown in Fig. 3, for which the first shrinkage step at 1340°C remains but the second shrinkage step now occurs at 1520°C. Since the ternary eutectic reaction remains the same, the difference in the onset temperature of the second shrinkage stage must be due to a different dissolution temperature of the nitride powders in the oxide melt. This difference could result from either the increase in nitrogen content or the change in the reaction kinetics in the presence of AlN. However, since no significant change in nitrogen content should arise from substituting a similar weight percentage of AlN for Si_3N_4, this shift is more likely due to a special effect of AlN on the reaction kinetics.

(B) Si_3N_4–AlN–Al_2O_3–Y_2O_3: To further explore the effect of AlN on hot pressing, several compositions on the Si_3N_4–

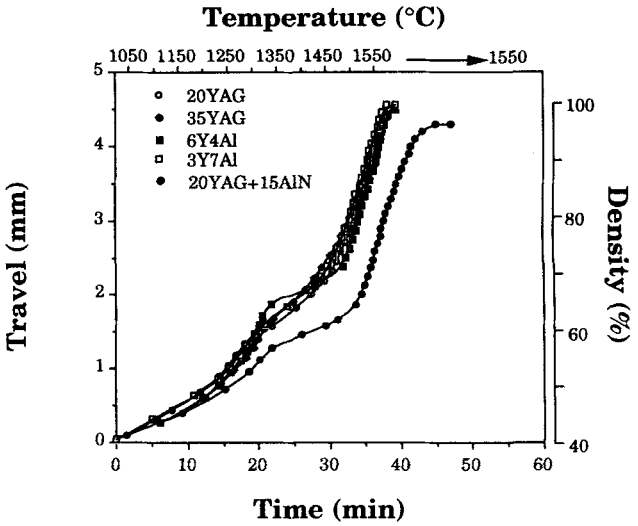

Fig. 3. Shrinkage curves for four materials on Si_3N_4–Al_2O_3–Y_2O_3 plane and one (20YAG + 15 AlN) with partial substitution of Si_3N_4 by AlN.

Al_2O_3:AlN–YN:3AlN plane were studied (Fig. 2). The compositions selected can be categorized into four groups: A, B, C, and D. Within each group, the ratio between Al_2O_3, Y_2O_3, and AlN is fixed. The materials in groups A and B are richer in AlN and Y_2O_3; groups C and D are richer in Al_2O_3.

We found materials within the same group to have essentially identical shrinkage curves regardless of composition. The shrinkage curves of group B materials are shown in Fig. 4 as an example. All the materials in this group have a similar first shrinkage step occurring at around 1350°C, and a second shrinkage step at 1540°C. Full density is obtained in about 15 min after the temperature reaches 1550°C. Similar shrinkage behavior with different temperature for the second shrinkage step was observed for other groups. For example, group C has a second step at 1470°C, as shown in Fig. 5, and group D at 1450°C, as shown in Fig. 6. (The first shrinkage step always occurs at ≈1350°C.) The contrast between the shrinkage behavior of different groups is summarized in Fig. 7, which includes compositions 1010 (group A), 0610 (group B), 0625 (group C), and 0650 (group D). The highest second-step temperature occurs at 1550°C in composition 1010, and the systematic decrease in this temperature from group A to B to C and to D is apparent. In all cases, the amount of shrinkage during the first step is approximately 4%, and that of the second step 40%. These values are similar to the ones observed for the Si_3N_4–Al_2O_3–Y_2O_3 system described in the previous section.

Based on the above observations it can be concluded that the shrinkage behavior of these materials depends strongly on the ratio of Al_2O_3:AlN/Y_2O_3:9AlN, which is fixed within each group. For the amount of (non-Si_3N_4) additives studied, which ranges from 17 wt% (0610) to 50 wt% (1145, 2135, and 0650), the shrinkage behavior is independent of the additive amount. In practice, all materials examined here can be hot-pressed to full density at 1550°C within 15 min with the exception of composition 1010, which reaches full density in about 30 min.

(2) Role of AlN

(A) Wettability: We found a significant difference between AlN and Si_3N_4 in their physical and chemical affinity to the oxide melt. This difference, revealed by a set of wetting experiments, proves critical to understanding the role of AlN on shrinkage characteristics. In these experiments, a certain amount of oxide powder mixture of the ternary eutectic composition was placed atop a substrate of hot-pressed Si_3N_4 or AlN pellet (not fully dense). They were heated in nitrogen using the same heating schedule as described in Section II(3) to various temperatures until the oxides melted to form a droplet on the substrate. (The holding time was 10 min at the desired temperature, and the atmosphere was 1 atm of N_2.) This is shown in Fig. 8. From such micrographs, the wetting angle of the oxide melt was measured and the results are plotted in Fig. 9. It can be seen that at 1420° and 1450°C when partial wetting occurs, the wetting angle on AlN is much smaller than on Si_3N_4. At 1500°C, the oxide melt wetted AlN fully so only the angle for Si_3N_4 could be measured.

(B) Reaction of AlN with Oxide Melt: Fast reaction between AlN and the oxide melt was evident from examination of the reaction layer beneath the oxide melt droplet in the wetting experiment. β'-SiAlON, 15R, AlN, Al_2O_3, and YAG were identified by XRD as shown in Fig. 10. An analysis of the positions of the β'-SiAlON lines gives lattice parameters close to those for β_{60}-SiAlON ($x = 4$).[29] Much less reaction was found between the oxide melt and Si_3N_4 at the same temperature and time (1420°C for 10 min). XRD analysis of phases in the hot-pressed materials also confirmed the faster reaction kinetics of AlN over Si_3N_4. For example, in a compact of 20YAG + 15AlN hot-pressed at 1400°C for 30 min, the peak ratio of Si_3N_4 ($2\bar{1}\bar{1}0$)/AlN(0002) is about 2, which is lower than the ratio (about 3) before hot pressing. Other phase examinations confirmed the same.

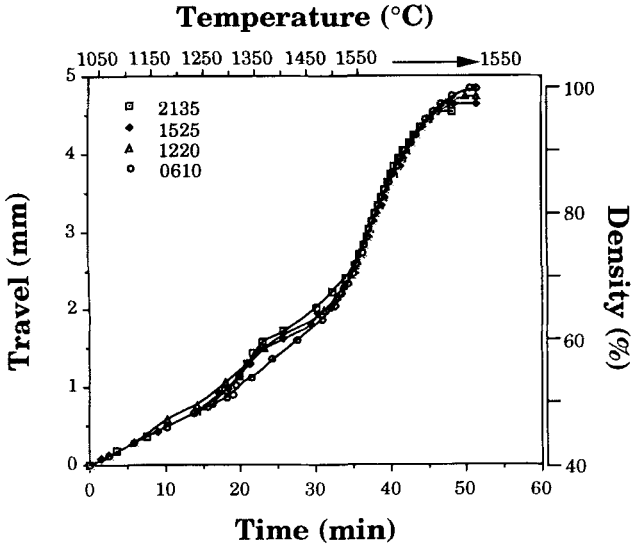

Fig. 4. Shrinkage curves for group B materials on Si_3N_4–Al_2O_3:AlN–YN:3AlN plane.

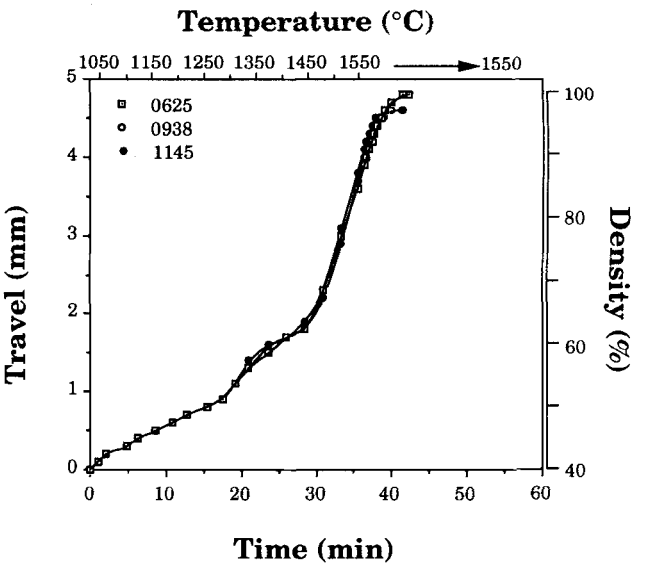

Fig. 5. Shrinkage curves for group C materials on Si_3N_4–Al_2O_3:AlN–YN:3AlN plane.

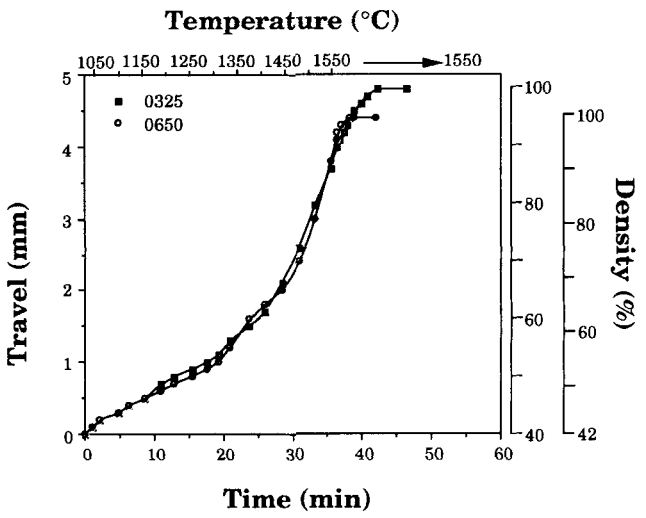

Fig. 6. Shrinkage curves for group D materials on Si_3N_4–Al_2O_3:AlN–YN:3AlN plane.

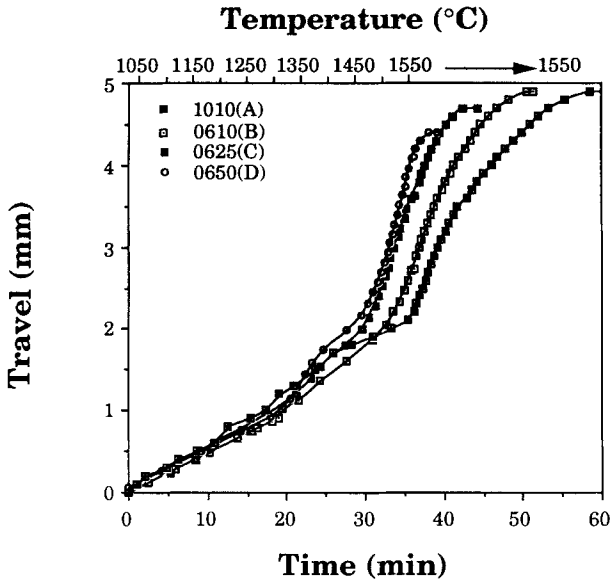

Fig. 7. Shrinkage curves of materials 1010 (A), 0610 (B), 0625 (C), and 0650 (D) on Si_3N_4–Al_2O_3:AlN–YN:3AlN plane.

(3) *Phase Evolutions*

We have already mentioned the presence of YAG and β_{60}-SiAlON in the reaction zone of ternary oxide eutectic and AlN. Extensive XRD analysis of the hot-pressed materials, some interrupted at temperatures below 1550°C, also revealed the following. First, all of the peaks for crystalline oxides in the starting powders disappeared above 1350°C, indicating rapid and complete melting. Second, YAG formed above 1350°C. This was true even when a special effort was made to effect rapid heating and cooling. Third, the initial β′-SiAlON formed had a composition higher in Al and O than the bulk. Fourth, in compositions rich in Al_2O_3 and Y_2O_3, AlN-polytypoids such as 15R and 12H were also found after hot pressing at 1550°C. Fifth, in compositions lean in Al_2O_3 and Y_2O_3 and intended to lie in the single-phase α′-SiAlON or (α′ + β′)-SiAlON range after complete reaction, the final β-SiAlON had a composition close to β_{10}-SiAlON. Sixth, the amount of YAG began to decrease at temperatures above 1450°C following the onset of the second shrinkage step. Finally, a substantial amount of unreacted α-Si_3N_4 remained after hot pressing in all materials except group D. A summary of the phase assemblage of four representative materials, one from each group, after hot pressing at 1550°C, is given in Table I. Also included in the table is the amount of glassy phase estimated from TEM and SEM.

We have performed extensive TEM analysis of the microstructure and microchemistry of some of these materials. The details of this analysis will be reported elsewhere. Here, only a

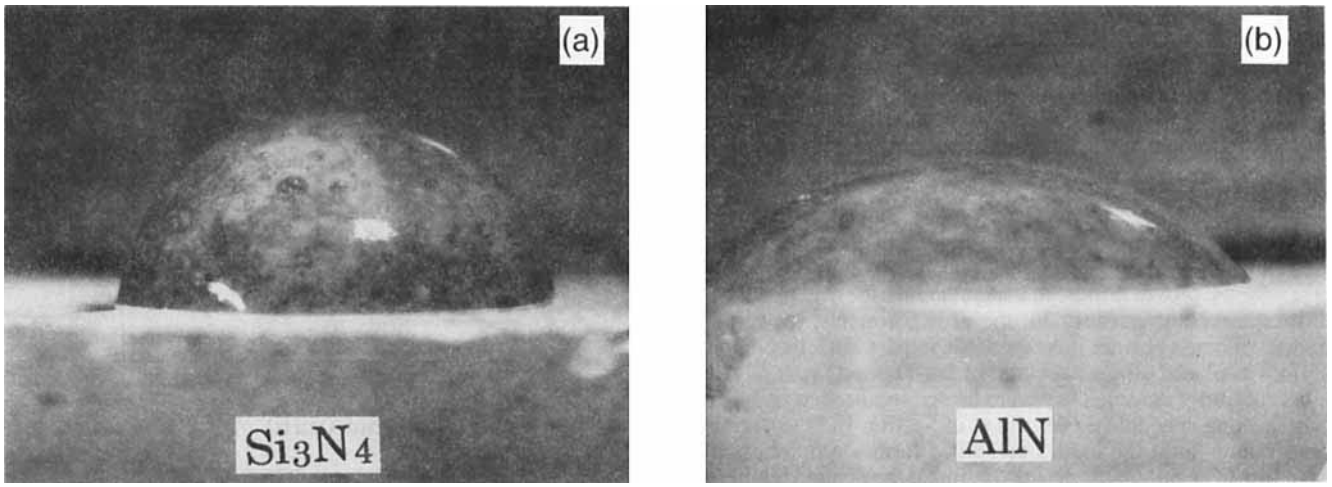

Fig. 8. SEM micrographs showing partial wetting of SiO_2–Al_2O_3–Y_2O_3 ternary eutectic melt on (a) Si_3N_4 and (b) AlN at 1420°C.

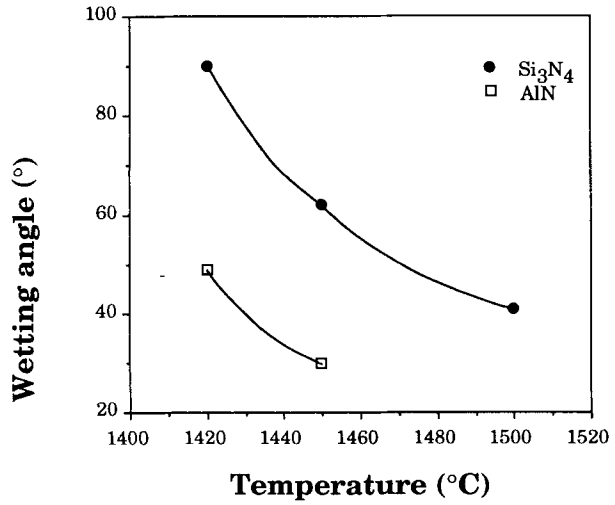

Fig. 9. Dependence of wetting angles on temperature for SiO_2–Al_2O_3–Y_2O_3 eutectic melt on Si_3N_4 and AlN.

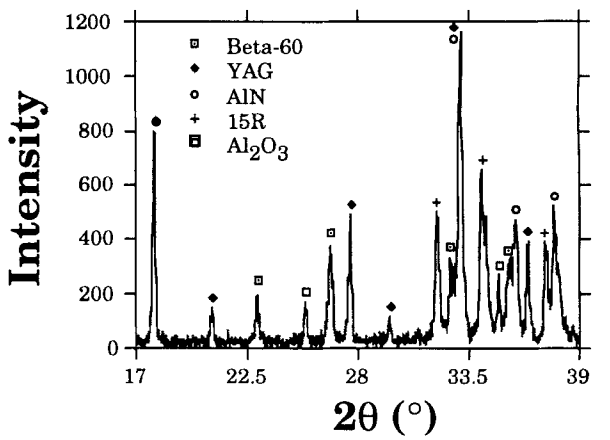

Fig. 10. XRD pattern of the interface between AlN and the SiO_2–Al_2O_3–Y_2O_3 eutectic melt (1420°C for 10 min).

Table I. Phase Assemblage

Material	Group	Equilibrium phase assemblage*	After hot-press/1550°C†	Glassy phase (vol%)
1010	A	α′	44%α, 56%α′	5
0610	B	α′ + β′	64%α, 27%α′, 9%β′	5
0625	C	β′ + 12H	56%α, 14%α′, 30%β′‡	10
0650	D	β′ + 15R	5%α, 95%β‡	13

*Per phase diagram. †1 h for A and 0.5 h for B–D. ‡YAG and AlN polytypoids (12H/15R) also found. The overall amount of both is less than 5%.

sample of the micrographs obtained from hot-pressed 0610 material (group B) is shown. Figure 11 is a TEM micrograph of an elongated β′-SiAlON grain. In the left center of the grain, a region of a different contrast can be seen. Using energy-dispersion X-ray analysis (EDS), the center left region was found to contain higher Al and O than the surrounding area and (according to chemical and diffraction analysis) was identified as β_{30}-SiAlON. This is in contrast with the remaining grain which was identified as $\approx \beta_{10}$-SiAlON. Further analysis of similar micrographs led us to conclude that the center left region was a seed crystal from which the elongated grain grew. A similar core-shell structure with a richer Al and O content in the core was also found in composition 0625 (group C) in which the core corresponded to $\approx\beta_{42}$-SiAlON. In 1010 (group A), only α-Si_3N_4 and α′-SiAlON and no β′-SiAlON was found.

IV. Discussion

(1) First Shrinkage Step

The first shrinkage step, in terms of the temperature and the shrinkage, is essentially independent of the powder compositions for all of the materials studied here. This can be understood by the ternary eutectic reaction. To estimate the shrinkage amount, which is around 4% (from 48 to 52%), we note that surface SiO_2 is around 2.5 vol%. For a eutectic melt composition of 44 wt% SiO_2, 22 wt% Al_2O_3, and 34 wt% Y_2O_3,[27] we then estimate the amount of the eutectic melt to be 4.1 vol%. If we assume that the shrinkage is due to the removal of liquid from the parent solid powder and redistribution of such liquid in the interstices, then the resultant densification can be calculated using the following equation:

$$D_f = D_i/(1 - V) \quad (1)$$

where D_i and D_f are the initial and final density and V is the volume percentage of the dissolved solid. This gives a 2% increase in density. The remaining 2% increase in density can be attributed to some slight improvement of packing efficiency.

(2) Second Shrinkage Step

The second shrinkage temperature is determined by the wetting condition of Si_3N_4/AlN, which precedes the dissolution of nitride powders. It also involves a large volume reduction from the very beginning. In materials 0650 and 1010 the initial shrinkage prior to the inflection point, which is below 1550°C and takes place within only 2 to 3 min, is already 15%. It seems likely that this is achieved by a massive particle rearrangement in the compact. Indeed, even in the later stage of second-step shrinkage, particle rearrangement is still predominant. This can be verified by plotting the isothermal shrinkage data, available from group B materials at 1550°C, in the manner of log $(L_0 - L)$ vs log $(t - t_0)$. (Here L and L_0 are current (at time t) and initial (at time t_0) lengths, respectively.) As shown in Fig. 12, the slope of the shrinkage curve plotted in this way is around 2/3, which is larger than the value 1/3 that would have been expected for the slower solution/reprecipitation process without massive particle rearrangement.[28] Thus, particle rearrangement commences in second-step shrinkage, and is responsible for a substantial portion of the volume reduction. It is likely that solution/reprecipitation is instrumental in this process by rounding off the sharp asperities of the powder particles. This will improve the mobility of particles and facilitate their sliding over each other under the combined action of applied stress and capillary force. The dissolution of nitride powders to make available an adequate amount of liquid is deemed essential for triggering this process.

(3) Role of AlN

In a powder compact containing AlN, Si_3N_4, and oxide melt, the presence of AlN with a smaller wetting angle will cause localization of the melt to AlN. If the amount of the melt is sufficiently small, this localization is complete and the compact is

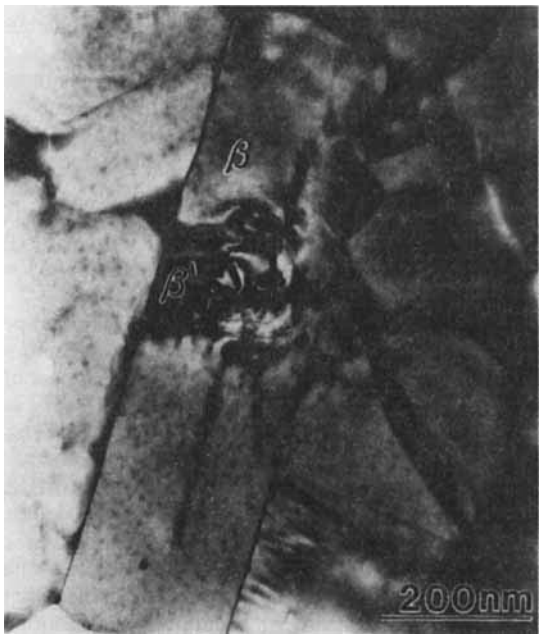

Fig. 11. TEM micrograph showing an elongated β′-SiAlON grain with a supersaturated β′-SiAlON seed at center left (material 0610).

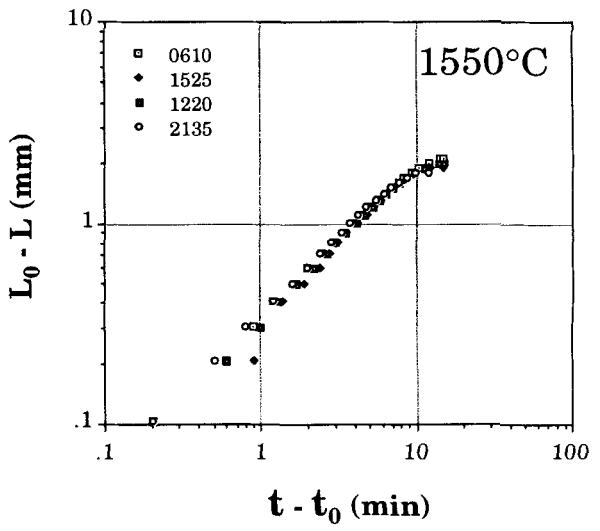

Fig. 12. Isothermal shrinkage curves in log $(L_0 - L)$ vs log $(t - t_0)$ for group B materials at 1550°C.

essentially "dry" except in isolated regions of AlN concentration. This liquid "trapping" situation is believed to occur in our materials in which the amount of ternary eutectic liquid is estimated to be 4 vol% and the amount of AlN varies from 8 to 23 wt%. Macroscopic shrinkage will have to be postponed until melt delocalization occurs at a higher temperature. This happens when the melt wets Si_3N_4, which then dissolves and provides more liquid to facilitate densification. In this way, AlN causes a delaying effect on the second shrinkage step.

The better wetting characteristics of AlN imply a higher chemical affinity between AlN and the oxide melt, as evidenced by the fast reaction between the two. Compared to Si_3N_4 dissolution, the preferential dissolution of AlN tends to increase the Al content of the liquid temporarily. Later, at a higher temperature when Si_3N_4 also dissolves, the Al concentration in the liquid is restored to the "bulk" value. We believe the transient supersaturation of Al causes the intial precipitation of Al(O)-rich β-SiAlON (e.g., β_{30} in 0610 and β_{42} in 0625), and the later restoration of overall average Al concentration is responsible for the subsequent precipitation of (equilibrium) β-SiAlON of a lower Al(O) content (e.g., β_{10}-SiAlON in 0610 and 1010). This sequence of reaction is qualitatively understandable from an inspection of the Si-Al-O-N phase diagram.[30]

(4) Reaction Pathway in Y-Si-Al-O-N System

The phase diagram of Y-Si-Al-O-N in the temperature range of 1350° and 1550°C is not complete in the current literature. However, from the ternary phase diagram of SiO_2–Al_2O_3–Y_2O_3,[27] the glass-forming region of Y-Si-Al-O-N at 1700°C,[31] the subsolidus phase relationship in the same,[32] and the solid solubility limits of the α′ phase on the Si_3N_4–YN:3AlN–Al_2O_3:AlN plane at 1800°C,[33] the following conclusions on the reaction pathway can be drawn. Three reactions are now identified.

(A) Ternary Oxide Eutectic Reaction (1340°C):

$$SiO_2 + Al_2O_3 + Y_2O_3 \longrightarrow (Si,Al,Y)_xO_y + YAG \qquad (2)$$

The presence of nitrogen is known to lower the eutectic temperature somewhat, as can be seen by the maximum expansion of the glass-forming region at about 15 equiv% N.[31] However, since the initial dissolution of AlN and Si_3N_4 is very limited, the suppression of eutectic temperature due to nitrogen is minimal. This is consistent with our observation. In addition, since the reaction is limited by the small amounts of SiO_2, the excess oxides tend to precipitate as YAG, which is the most likely compound in the composition intermediate between Al_2O_3 and Y_2O_3.[27]

(B) Initial Nitride Precipitation (1420–1550°C):

$$(Si,Al,Y)_xO_y + AlN \longrightarrow \beta'\text{-SiAlON (supersaturated)} + (Si,Al,Y)_x(O,N)_y \qquad (3)$$

The initial precipitation follows AlN dissolution and has a β-SiAlON composition rich in Al and O. For this reaction, our phase analysis indicates that YAG is initially compatible with the oxynitride liquid and β′-SiAlON. In the phase diagram,[31,32] we envision a compatibility cone bounded by supersaturated β′-SiAlON, YAG, and a line of liquid solution on the surface of the oxynitride glass-forming region. (Toward the oxide triangle, there should be another compatibility region bounded by YAG and a surface of the liquid-forming region.) The composition line connecting AlN and the ternary oxide eutectic then determines the pertinent composition in the reaction zone. This composition initially traverses from the liquid-YAG compatible region and later enters the β′-YAG-liquid cone. In this way, AlN dissolution triggers the precipitation of superaturated β′-SiAlON. This reaction continues until Si_3N_4 dissolution.

(C) Secondary Nitride Precipitation (above 1470°C):

$$(Si,Al,Y)_x(O,N)_y + Si_3N_4 + YAG \longrightarrow \beta_{10-60} + \alpha' \qquad (4)$$

With complete dissolution of starting powders, the final composition, by design, falls on the α′ plane (Si_3N_4–YN:3AlN–Al_2O_3:AlN). This, however, was usually not achieved in our study as evidenced by the presence of residual α-Si_3N_4 even after complete densification at 1550°C. Thus, the actual composition is somewhat away from the Si_3N_4 corner on the α′ plane. Referring to the phase diagram,[32,33] we find that at the solubility limit α′-SiAlON is in equilibrium with β_{10}-SiAlON. A compatibility tetrahedron α′-β_{10}-YAG-12H as well as other similar compatibility relationships (β_{10}-β_{25}-12H-YAG, β_{25}-15R-12H-YAG, and β_{25}-β_{60}-15R-YAG) may prevail depending on the actual composition on the plane. In general, the secondary precipitation tends to form β′-SiAlON of a lower (Al,O) content than the initial precipitation.

In reaching the final equilibrium, much of YAG resorbs to provide Al (and some Y) to the SiAlON precipitates. (Indeed, we found YAG to dissolve toward the end of α′/β′-SiAlON precipitation.) Resorbtion of supersaturated β′-SiAlON would also occur in some compositions. In other compositions where supersaturated β′-SiAlON was already incorporated as the core of the SiAlON grains, it would tend to remain because of the sluggish kinetics of solid-state reaction. In addition, although β_{60}-SiAlON was found on the AlN substrate in the wetting experiment (Fig. 10), the composition richest in AlN, 1010, did not contain any β_{60}-SiAlON after hot pressing according to TEM. Thus, the supersaturated β′-SiAlON is transient and not compatible with the final phase assemblage.

We should caution the readers that our experiments involving complex oxides and nitrides are generally kinetically determined phenomena. Thus, they are not entirely bound by equilibrium considerations and do not always follow phase diagrams. Nevertheless, the above synopsis seems to be in good accord with our observations. This probably implies that equilibrium considerations, when aided by kinetic arguments, still largely dictate the directions of reaction pathways.

(5) Processing Considerations

For materials on the α′-plane, the composition of additives can be represented as $\xi(9AlN{:}Y_2O_3) + (1 - \xi)(AlN{:}Al_2O_3)$. (An alternative representation in terms of (3YN:3AlN) and ($AlN{:}Al_2O_3$) would give similar results but with ξ scaled differently.) Using this representation, the dependence of the starting temperature of the second shrinkage step is seen in Fig. 13. Here, the points at $\xi = 0.5, 0.3, 0.12, 0.06$ are, respectively, group A, B, C, D, while the points at $\xi = 1$ and 0 are taken from Refs. 14, 26, and 34. The point of $\xi = 0$ may be regarded as an exception, since it represents β′-SiAlON composition and lacks Y_2O_3 in the starting composition, hence a higher eutectic temperature of the oxide powders. Once the composition moves into finite ξ, the hot pressing temperature increases monotonically with ξ until it reaches the Si_3N_4–Y_2O_3:9AlN line ($\xi = 1$). The hot pressing temperature for the latter composition usually exceeded 1650°C. The lowest hot pressing temperature for compositions on the α′ plane is thus around 1450°C. Indeed, we have successfully hot-pressed materials 0625 ($\xi = 0.12$) and 0650 ($\xi = 0.06$) to full density at 1500°C. The material 0625 reached full density within 20 min and the material 0650 within 5 min.

Such compositional dependence of hot pressing temperature is believed to be related to the viscosity of the melt and/or other aspects of the kinetics. As shown in Table I, the amount of unreacted α-Si_3N_4 decreases from group B to C to D. (The amount of α-Si_3N_4 in material 1010 is less because of the longer hot pressing time.). In the same sequence, the N/O ratio and hence viscosity[31] also decrease. Thus, the precipitation of SiAlON phases is empirically correlated to α-Si_3N_4 dissolution, melt viscosity, and N/O ratio. However, since full density can be achieved well in advance of complete α-Si_3N_4 dissolution, the main role of the dissolution/precipitation in densification probably lies in rounding off asperities on powders to improve their mobility initially, and in liquid-enhanced sintering to eliminate pores subsequently. As the amount of transient liquid initially increases, then decreases, the densification rate apparently

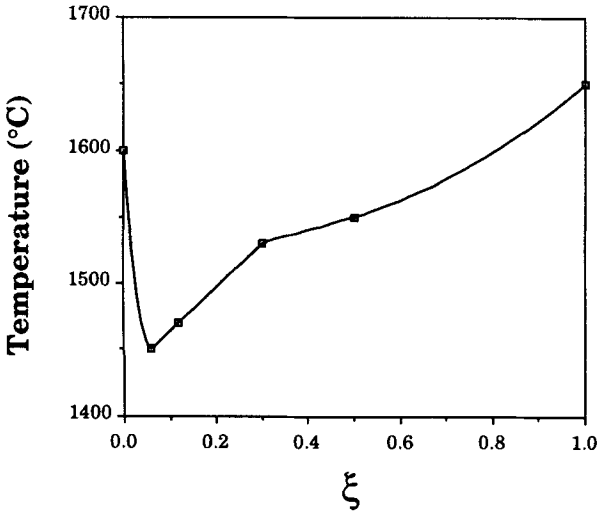

Fig. 13. Hot pressing temperature vs ξ value for compositions on the Si_3N_4–Al_2O_3:AlN–YN:3AlN plane.

follows the same trend. Phase transformation from α-Si_3N_4 to α′/β′-SiAlON is merely coincidental in the above sequence.

Finally, we note that our hot pressing temperatures are considerably lower than typically reported for SiAlON ceramics.[4,14–20] This is mostly due to a more uniform mixture of finer powders which were present in the submicrometer sized forms. The combination of a more uniform mixture, finer powders, and an applied pressure allowed the manifestation of distinct shrinkage steps beginning at 1350°C and complete densification at 1550°C. The relatively low temperature and short time used, in turn, allowed us to capture early events along the reaction pathway toward forming SiAlON phases. The resultant materials containing a substantial amount of unreacted α-Si_3N_4 and submicrometer SiAlON phases are amenable to superplastic forming to large strains in biaxial punch stretching.[24,35]

V. Conclusions

(1) Densification of SiAlON using Si_3N_4, AlN, Al_2O_3, and Y_2O_3 proceeds in two steps. At 1340°C, a ternary eutectic oxide melt of SiO_2, Al_2O_3, and Y_2O_3 forms and a small shrinkage occurs. This is followed by nitride dissolution at temperatures above 1450°C causing a massive particle rearrangement and further densification by solution/reprecipitation.

(2) AlN plays an essential role in directing the kinetic pathway of the second step. With better wettability, AlN initially traps the oxide melt to prevent Si_3N_4 dissolution. Preferential dissolution of AlN at 1450°C enriches the melt composition in Al, triggering transient precipitation of supersaturated β′-SiAlON.

(3) Si_3N_4, which dissolves at above 1470°C in the presence of AlN, dilutes the Al concentration in the melt. Although the amounts of α′/β′-SiAlON formed and α-Si_3N_4 dissolved depend on the composition and generally decrease with N/O ratio, full densification is readily achieved without complete dissolution/precipitation.

(4) $Y_3Al_5O_{12}$ is compatible with ternary oxide melt and all of the intermediate and final phase assemblages. It initially forms to absorb excess Al_2O_3 and Y_2O_3 upon melt formation, then gradually resorbs to provide Al and O (also Y in some cases) to precipitating SiAlON phases.

References

[1]L. J. Bowen, T. G. Carruthers, and R. J. Brook, "Hot-Pressing of Si_3N_4 with Y_2O_3 and Li_2O as Additives," *J. Am. Ceram. Soc.*, **61** [7–8] 335–39 (1978).

[2]L. J. Bowen, R. J. Weston, T. G. Carruthers, and R. J. Brook, "Hot Pressing and the α–β Phase Transformation in Silicon Nitride," *J. Mater. Sci.*, **13**, 341–50 (1978).

[3]G. R. Terwilliger and F. F. Lange, "Hot-Pressing Behavior of Si_3N_4," *J. Am. Ceram. Soc.*, **57** [1] 25–29 (1974).

[4]H. C. Yeh, W. A. Sanders, and J. L. F. Luttner, "Pressure Sintering of Si_3N_4–Al_2O_3 (SiAlON)," *J. Am. Ceram. Soc.*, **56** [2] 189–93 (1977).

[5]M. Mitomo, "Pressure Sintering of Si_3N_4," *J. Mater. Sci.*, **11**, 1103–107 (1976).

[6]P. Drew and M. H. Lewis, "The Microstructures of Silicon Nitride Ceramics During Hot-Pressing Transformations," *J. Mater. Sci.*, **9**, 261–69 (1974).

[7]O. L. Krivanek, T. M. Shaw, and G. Thomas, "The Microstructure and Distribution of Impurities in Hot-Pressed and Sintered Silicon Nitrides," *J. Mater. Sci.*, **62** [11–12] 585–90 (1979).

[8]D. R. Clark, N. J. Zaluzec, and R. W. Carpenter, "The Intergranular Phase in Hot-Pressed Silicon Nitride: I, Elemental Composition," *J. Mater. Sci.*, **64** [10] 601–607 (1981).

[9]C. C. Ahn and G. Thomas, "Microstructure and Grain-Boundary Composition of Hot-Pressed Silicon Nitride with Yttria and Alumina," *J. Am. Ceram. Soc.*, **66** [1] 14–17 (1983).

[10]F. F. Lange, "Phase Relations in the System Si_3N_4–SiO_2–MgO and Their Interrelation with Strength and Oxidation," *J. Am. Ceram. Soc.*, **61** [1–2] 53–56 (1978).

[11]F. F. Lange, "High Temperature Strength Behavior of Hot-Pressed Si_3N_4: Evidence for Sub-Critical Crack Growth," *J. Am. Ceram. Soc.*, **62** [3–4] 222–23 (1979).

[12]D. P. Thompson, "The Crystal Chemistry of Nitrogen Ceramics," *Mater. Sci. Forum*, **47**, 21–24 (1989).

[13]G. Z. Cao and R. Metselaar, "α′-SiAlON Ceramics: A Review," *Chem. Mater.*, **3**, 242–52 (1991).

[14]E. Kokmeijer and R. Metselaar, "Hot Pressing of SiAlON"; pp. 1.351–1.355 in *Euro-Ceramics*, Vol. 1. Edited by G. de With, R. A. Terpstra, and R. Metselaar. Elsevier Applied Science, London, U.K., 1989.

[15]M. Kuwabara, M. Benn, and F. L. Riley, "The Reaction Hot Pressing of Compositions in the System Al-Si-N-O Corresponding to β′-SiAlON," *J. Mater. Sci.*, **15**, 1407–16 (1980).

[16]M. N. Rahaman, F. L. Riley, and R. J. Brook, "Mechanisms of Densification During Reaction Hot-Pressing in the System Si-Al-O-N," *J. Am. Ceram. Soc.*, **63** [11–12] 648–53 (1980).

[17]M. H. Lewis, B. D. Powell, P. Drew, R. J. Lumby, B. North, and A. J. Taylor, "The Formation of Single-Phase Si-Al-O-N Ceramics," *J. Mater. Sci.*, **12**, 61–74 (1977).

[18]M. Rahaman and F. L. Riley, "Densification Behavior During Reaction Hot-Pressing of Compositions in the β′-SiAlON System," *Proc. Brit. Ceram. Soc.*, **31**, 63–70 (1981).

[19]M. Benn, M. Kuwabara, and F. L. Riley, "Reactive Hot-Pressing of Phases in the System $Si_{6-z}Al_zO_zN_{8-z}$"; pp. 119–26 in *Science of Ceramics 9*. Edited by D. E. Taylor. British Ceramic Society, London, U.K., 1977.

[20]M. Haviar and P. L. Hansen, "Hot Pressing and α–β′ Phase Transformation of Compositions Corresponding to β′-SiAlON," *J. Mater. Sci.*, **25**, 992–96 (1990).

[21]S. Boskovic, J. L. J. Gauckler, G. Petzow, and T.-Y. Tien, "Reaction Sintering Forming β-Si_3N_4 Solid Solutions in the System Si,Al/N,O I: Sintering of SiO_2–AlN Mixtures," *Powder Metall. Int.*, **9** [4] 185–89 (1977).

[22]S. Boskovic, J. L. J. Gauckler, G. Petzow, and T.-Y. Tien, "Reaction Sintering Forming β-Si_3N_4 Solid Solutions in the System Si,Al/N,O II: Sintering of Si_3N_4–SiO_2–AlN Mixtures," *Powder Metall. Int.*, **10** [4] 180–85 (1978).

[23]S. Boskovic, J. L. J. Gauckler, G. Petzow, and T.-Y. Tien, "Reaction Sintering Forming β-Si_3N_4 Solid Solutions in the System Si,Al/N,O III: Sintering of Si_3N_4–AlN–Al_2O_3 Mixtures," *Powder Metall. Int.*, **11** [4] 169–71 (1979).

[24]I-W. Chen and L. A. Xue, "Development of Superplastic Structural Ceramics," *J. Am. Ceram. Soc.*, **73** [9] 2585–609 (1990).

[25]I-W. Chen and S. L. Hwang, "Shear Thickening Creep in Superplastic Silicon Nitride," *J. Am. Ceram. Soc.*, **75** [5] 1073–79 (1992).

[26]X. Wu and I-W. Chen, "Exaggerated Texture and Grain Growth in a Superplastic SiAlON," *J. Am. Ceram. Soc.*, **75** [10] 2733–41 (1992).

[27]E. M. Levin, C. R. Robbins, and H. F. McMurdie, *Phase Diagrams for Ceramists, 1969 Supplement*; Fig. 2586, p. 165. Edited by M. K. Reser. American Ceramic Society, Columbus, OH, 1969.

[28]W. D. Kingery, J. M. Woulbroun, and F. R. Charvat, "Effects of Applied Pressure on Densification During Sintering in the Presence of a Liquid Phase," *J. Am. Ceram. Soc.*, **46** [8] 391–95 (1963).

[29]M. Haviar and O. Johannsen, "Unit-Cell Dimensions of β′-Sialons," *Adv. Ceram. Mater.*, **3** [4] 405–407 (1988).

[30]I. K. Naik, L. J. Gauckler, and T.-Y. Tien, "Solid–Liquid Equilibria in the System Si_3N_4–AlN–SiO_2–Al_2O_3," *J. Am. Ceram. Soc.*, **61** [7–8] 332–35 (1978).

[31]S. Hampshire, "Oxynitride Glasses and Glass Ceramics"; pp. 93–104 in Materials Research Society Symposia Proceedings, Vol. 287, *Silicon Nitride Ceramics: Scientific and Technological Advances*. Edited by I-W. Chen, P. F. Becher, M. Mitomo, G. Petzow, and T.-S. Yen. Materials Research Society, Pittsburgh, PA, 1993.

[32]W.-Y. Sun, T.-Y. Tien, and T.-S. Yen, "Subsolidus Phase Relationships in Part of the System Si,Al,Y/N,O: The System Si_3N_4–AlN–YN–Al_2O_3–Y_2O_3," *J. Am. Ceram. Soc.*, **76** [11] 2753–58 (1991).

[33]W.-Y. Sun, T.-Y. Tien, and T.-S. Yen, "Solubility Limits of α′-Sialon Solid Solutions in the System Si,Al,Y/N,O," *J. Am. Ceram. Soc.*, **74** [10] 2547–50 (1991).

[34]M. Mitomo, N. Kuramoto, and H. Suzuki, "The Formation of Single Phase β-SiAlON"; pp. 463–67 in *Proceeding of the International Symposium on Factors in Densification and Sintering of Oxide and Non-oxide Ceramics*. Edited by S. Somiya and S. Saito. Association for Science Document Information, Tokyo, Japan, 1978.

[35]S.-L. Hwang, "Fabrication, Microstructural Characterization, and Deformation of Superplastic Sialon Ceramics"; Ph.D. Dissertation. University of Michigan, Ann Arbor, MI, 1992. □